

Timothy J. Gundert

Department of Biomedical Engineering,
Marquette University,
1515 West Wisconsin Avenue,
Milwaukee, WI 53233

Alison L. Marsden

Weiguang Yang

Mechanical and Aerospace
Engineering Department,
University of California San Diego,
9500 Gillman Drive,
La Jolla, CA 92093

John F. LaDisa Jr.¹

Department of Biomedical Engineering,
Marquette University,
1515 West Wisconsin Avenue,
Milwaukee, WI 53233;
Department of Medicine,
Division of Cardiovascular Medicine,
Medical College of Wisconsin,
8701 Watertown Plank Road,
Milwaukee, WI 53226;
Department of Pediatrics,
Division of Pediatrics,
Children's Hospital of Wisconsin,
9000 W. Wisconsin Avenue,
Wauwatosa, WI 53226,
e-mail: john.ladisa@marquette.edu

Optimization of Cardiovascular Stent Design Using Computational Fluid Dynamics

Coronary stent design affects the spatial distribution of wall shear stress (WSS), which can influence the progression of endothelialization, neointimal hyperplasia, and restenosis. Previous computational fluid dynamics (CFD) studies have only examined a small number of possible geometries to identify stent designs that reduce alterations in near-wall hemodynamics. Based on a previously described framework for optimizing cardiovascular geometries, we developed a methodology that couples CFD and three-dimensional shape-optimization for use in stent design. The optimization procedure was fully-automated, such that solid model construction, anisotropic mesh generation, CFD simulation, and WSS quantification did not require user intervention. We applied the method to determine the optimal number of circumferentially repeating stent cells (N_C) for slotted-tube stents with various diameters and intrastent areas. Optimal stent designs were defined as those minimizing the area of low intrastent time-averaged WSS. Interestingly, we determined that the optimal value of N_C was dependent on the intrastent angle with respect to the primary flow direction. Further investigation indicated that stent designs with an intrastent angle of approximately 40 deg minimized the area of low time-averaged WSS regardless of vessel size or intrastent area. Future application of this optimization method to commercially available stent designs may lead to stents with superior hemodynamic performance and the potential for improved clinical outcomes.
[DOI: 10.1115/1.4005542]

Keywords: computational fluid dynamics, coronary artery disease, cardiovascular stent, optimization, wall shear stress

1 Introduction

The use of cardiovascular stents has undoubtedly transformed the treatment of coronary artery disease, however, restenosis after stent implantation remains a significant clinical issue [1,2]. Although drug-eluting stents (DESs) have decreased the incidence of restenosis compared to bare metal stents (BMSs), retrospective studies of DESs still report restenosis rates as high as 6–8% [3,4] and incomplete endothelialization that can be associated with thrombus formation in some cases [5–7]. Previous studies indicate a correlation between altered near-wall hemodynamics, specifically low wall shear-stress (WSS), and neointimal hyperplasia that leads to restenosis [8,9]. Low WSS also correlates with areas of inhibited endothelial cell migration onto stent surfaces [10]. Since stent geometry is known to affect the distribution of the WSS imparted on the vessel wall [11–14], determining the geometry that minimizes stent-induced low WSS could further improve clinical outcomes.

Computational fluid dynamics (CFD) is a valuable tool for analyzing the hemodynamic effects of stent geometry since associated indices (i.e., pressure, velocity, WSS, etc.) are difficult to quantify

in vivo. Computational studies of idealized stent geometries have shown that thinner struts and those more aligned with the primary flow direction decrease the amount of low WSS at the arterial wall [11,15]. Other studies have used CFD to compare various commercial stent designs [12–14,16]. While these studies provide useful insights for improving stent design, they only analyzed a small number of possible stent geometries in order to identify the general trends that govern stent design.

In contrast, incorporating a shape optimization algorithm with a proven convergence theory into the design process allows engineers to systematically identify the most favorable designs. Previous CFD optimizations of coronary stent design have been limited to two-dimensional stent models or optimizations of a single stent cell [17–19]. The objective of this investigation was to develop a fully automated framework for designing hemodynamically optimal coronary stents using CFD of complete, three-dimensional stent geometries. Traditional gradient-based optimization methods often require invasive changes to the solver code, therefore limiting their potential applications. In this work, the use of a derivative-free method facilitated the development of a flexible and efficient optimization framework. The utility of this framework was demonstrated by optimizing the number of circumferentially repeating stent cells (N_C) for various slotted-tube stents, since this simple design parameter could not be optimized using previously mentioned two-dimensional and single cell methods. During the course of this investigation, it was hypothesized that the strut angle relative to the primary direction of flow dictates the optimal value of N_C .

¹Corresponding author.

Contributed by the Bioengineering Division of ASME for publication in the JOURNAL OF BIOMECHANICAL ENGINEERING. Manuscript received June 21, 2011; final manuscript received December 3, 2011; accepted manuscript posted January 23, 2012; published online February 8, 2012. Assoc. Editor: Ender A. Finol.

We therefore performed a second set of optimizations to determine if the optimal strut angle correlates with the optimal values of N_C computed in the first optimization study. For both optimizations, the stent design that minimized the area of low time-average WSS (TAWSS) was defined as optimal.

2 Methods

2.1 Overview of Model Generation and Parameterization.

Generic slotted-tube stents, similar to the Palmaz-Schatz design, were modeled in an expanded state using SolidWorks (Concord, MA). The models were parameterized such that the stent cell axial length (l_a), the circumferential distance between adjacent struts (l_c), and the intrastrut angle (θ) could be altered (Fig. 1). A custom software program was written using the SolidWorks application programming interface to automatically generate solid models of stent designs for a given set of parameters. Each parameter set contained only two of the previously mentioned parameters, since the three parameters are not independent.

The stent strut thickness and intrastrut area were explicitly defined to prevent the optimization routine from pursuing infeasible stent designs, since the objective of minimizing low TAWSS within a vessel is ideally met by a stent design with negligible strut thickness and large intrastrut areas if these parameters are not kept constant. This intuition was confirmed by the preliminary optimizations before the strut width and thickness were defined as $100\ \mu\text{m}$, which is similar to the size of an average stent. The intrastrut area of commercial closed-cell stents varies between $1\ \text{mm}^2$ and $3\ \text{mm}^2$, and an ideal area is not known. Therefore, optimizations were performed with intrastrut areas of $1\ \text{mm}^2$, $2\ \text{mm}^2$, and $3\ \text{mm}^2$ (Fig. 1) to examine the effect of this parameter on optimal stent design within the range of commercial stents.

Generated stent models were virtually implanted into the vessels using a Boolean subtraction operation [16]. Vessels were modeled with a stent to artery ratio of 1.1:1 [20] and a length of 32 mm. The expanded region of the vessels was 18 mm in length with a 2 mm tapered section connecting the stented and unstented regions [14]. To analyze the effect of the vessel diameter on opti-

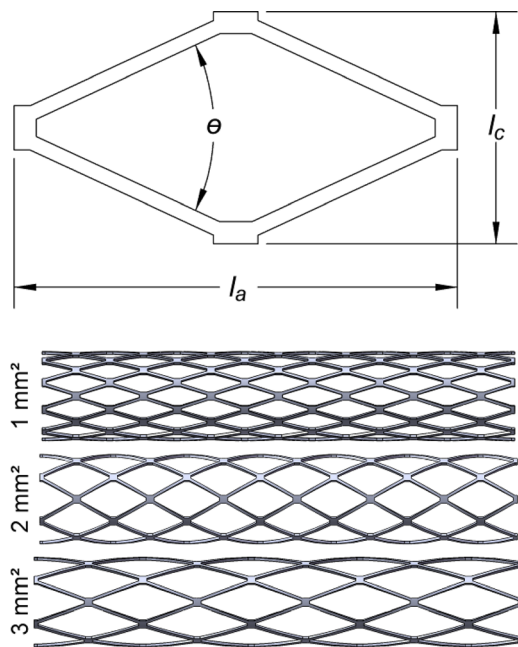


Fig. 1 (top) Parameterized drawing of a stent cell which is characterized by the cell axial length (l_a), circumferential distance between struts (l_c), and intrastrut angle (θ). **(bottom)** Examples of three stent models with different intrastrut areas, shown to the left of each model.

mal stent designs, all optimizations were performed in both small (SV) and large vessels (LV) with diameters of 2.25 mm and 3.0 mm, corresponding to stent diameters of 2.475 mm and 3.3 mm, respectively.

2.2 Stent Models for Optimizing the Number of Circumferentially Repeating Stent Cells. The optimal value of N_C was computed for each combination of vessel size and intrastrut area for a total of six stent design optimizations. To define the cell geometry for a given N_C , l_c was first computed based on the stent diameter and N_C . Subsequently, l_a was computed to maintain a constant intrastrut area of either $1\ \text{mm}^2$, $2\ \text{mm}^2$, or $3\ \text{mm}^2$. The cell geometry was then circumferentially and axially replicated to create a complete stent model with a target length of 18 mm.

2.3 Stent Models for Optimizing the Intrastrut Angle. The model construction method described in the previous section could not be used to optimize θ because the constraints of an integer number of circumferentially repeating cells and a constant intrastrut area only allows for the creation of stent models with discrete θ values. Instead, stent models were created in which θ was a continuous variable and, consequently, N_C was also allowed to be a continuous variable. Models created using this approach had a repeating strut configuration that propagated around the circumference of the vessel, but did not necessarily meet to form a continuous pattern. While this approach did not create feasible stent designs, it provided a means of investigating the optimal intrastrut angle with fine detail. To create a stent model for a given θ , l_a was first computed to maintain a constant intrastrut area of either $1\ \text{mm}^2$, $2\ \text{mm}^2$, or $3\ \text{mm}^2$ and then a complete stent model was generated with a target length of 18 mm, as previously discussed. As with the optimization of the number of repeating circumferential units, the optimal θ was computed for each combination of vessel size and intrastrut area.

2.4 Computational Simulations. Following model generation (Figs. 2(a) and 2(b)), the solid model of the implanted stent was discretized into a finite element mesh using MeshSim (Simmetrix, Clifton Park, NY). Highly anisotropic meshes were generated such that WSS could be well resolved without necessitating intense computational cost (Fig. 2(c)). A more coarse mesh was prescribed in the proximal and distal unstented regions of the vessel, with a finer mesh density prescribed for the stented region, and a very fine mesh density prescribed in the intrastrut regions that are later quantified as part of the optimization routine. Meshes ranged in size from 3.0 to 6.3×10^6 elements, depending on the stent design.

In prescribing boundary conditions to each model, the artery was assumed to be rigid and a no-slip boundary condition was prescribed on the vessel and stent surfaces. Blood was assumed to be a Newtonian fluid with a density of $1.06\ \text{g/cm}^3$ and a viscosity of 4 cP. A time-varying canine left-anterior descending coronary artery flow waveform [21] with characteristics similar to those found in humans was imposed at the model inlet using a Womersley velocity profile (Fig. 2(d)). The inflow rate was not scaled for different diameter vessels. Outlet boundary conditions were prescribed using three-element Windkessel approximations, consisting of characteristic (R_c) and distal (R_d) resistances, as well as a capacitance (C) term, to replicate the physiologic impedance of the downstream vasculature (Fig. 2(d)), as previously described [22–24].

CFD simulations were run using an in-house stabilized finite element solver with a commercial linear solver component LESLIB (Altair Engineering, Troy, MI) to solve the time-dependent Navier-Stokes equations. The time step was chosen for a Courant, Friedrichs, and Lewy condition <1 . Simulations were run until the outlet pressure and flow were periodic; defined as a maximum error between equivalent points in successive cardiac cycles $<1\ \text{mm Hg}$ and $<1\ \text{mm}^3/\text{s}$. The TAWSS was then

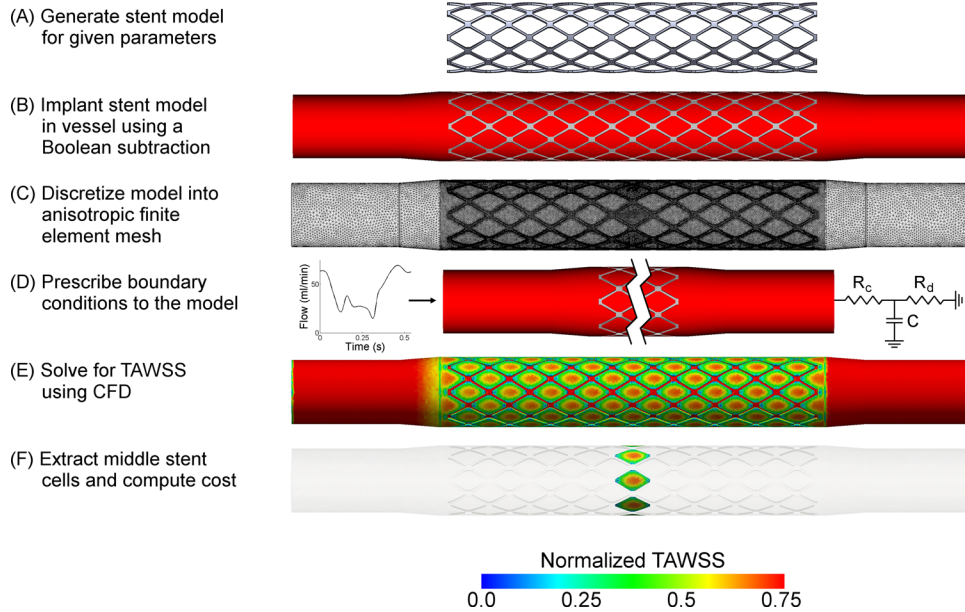


Fig. 2 Description of the steps necessary for evaluating a stent design. The TAWSS is shown normalized to the average TAWSS in the proximal unstented region of the model.

computed over the last cardiac cycle as previously described [25] (Fig. 2(e)). Cells in the middle of the stented region were extracted for subsequent evaluation in the optimization routine (Fig. 2(f)).

2.5 Cost Function. Previous studies correlating local blood flow patterns to endothelialization, neointimal hyperplasia growth, and the progression of atherosclerosis support the hypothesis that there exists a homeostatic level of the WSS that blood vessels prefer. In particular, deviations from homeostatic levels of the WSS cause vascular remodeling [26,27]. We therefore chose a cost function (J) which aims to maximize TAWSS in the stented region (\overline{TAWSS}_{IS}) relative to TAWSS in an unstented portion of the vessel (\overline{TAWSS}_{US}). Formulated as a minimization, the cost function is therefore

$$J = 1 - \frac{\overline{TAWSS}_{IS}}{\overline{TAWSS}_{US}} \quad (1)$$

where \overline{TAWSS}_{IS} is computed by integrating TAWSS over the intra-stent surfaces (s), normalized to the area of those surfaces

$$\overline{TAWSS}_{IS} = \frac{\int_s TAWSS ds}{\int_s ds} \quad (2)$$

Only the middle stent cells (Fig. 2(f)) were used to compute \overline{TAWSS}_{IS} to mitigate the effects of slightly varying stent lengths and flow disruptions near the ends of the stented regions. The value of \overline{TAWSS}_{US} was computed as

$$\overline{TAWSS}_{US} = \frac{4\mu Q}{\pi r^3} \quad (3)$$

where Q is the mean flow, μ is the viscosity, and r is the vessel radius. A custom software program that used the Visualization Toolkit (VTK, Kitware, Clifton Park, NY) libraries was written to compute the cost function.

2.6 Optimization Routine. The surrogate management framework (SMF), previously described by Booker et al. and applied to cardiovascular engineering problems by Marsden et al. was used to determine optimal stent designs [28,29]. The general formulation of the optimization is given by

$$\begin{aligned} &\text{minimize } J(\mathbf{x}) \\ &\text{subject to } \mathbf{x} \in \Omega \end{aligned} \quad (4)$$

where J represents the cost function for a given vector of parameters \mathbf{x} (i.e., the number of the circumferentially repeating cell or the intrastrut angle) within the domain Ω . The SMF framework is a derivative-free optimization algorithm that relies on pattern search theory for convergence of the cost function to a local minimum. The method restricts all parameters to lie on a discrete parameter mesh that may be refined to increase the resolution of the parameter space as the algorithm progresses. Our implementation of the SMF algorithm uses a mesh adaptive direct search (MADS) polling method, which has a stronger convergence theory compared to previous generalized pattern search methods [30]. Due to the large computational effort required for evaluating the cost function for a given set of parameter values, the SMF uses a surrogate function to predict the location of the local minimum, which increases the efficiency of the optimization [28]. Though various surrogate functions can be used with the SMF method, our implementation incorporates a Kriging surrogate function using the MATLAB DACE package [31] to easily extend this approach to multiple dimensions and avoid the problems of overshoot found in polynomial interpolation.

The SMF optimization algorithm is schematically illustrated in Fig. 3. The algorithm is initialized using Latin hypercube sampling (LHS) to generate a well-distributed set of input variables, or trial points, over the discrete parameter space [32]. Stent models are constructed and evaluated for each trial point and the resulting cost function values are used to construct the initial surrogate function.

The optimization loop consists of two fundamental steps, SEARCH and POLL. During the SEARCH step, the surrogate function is used to predict the location of parameters that minimize the cost function. If evaluation of the trial points generated by the SEARCH steps improves the current best point, another SEARCH steps ensues. After every SEARCH step, the surrogate function is updated to incorporate all new cost function values. If

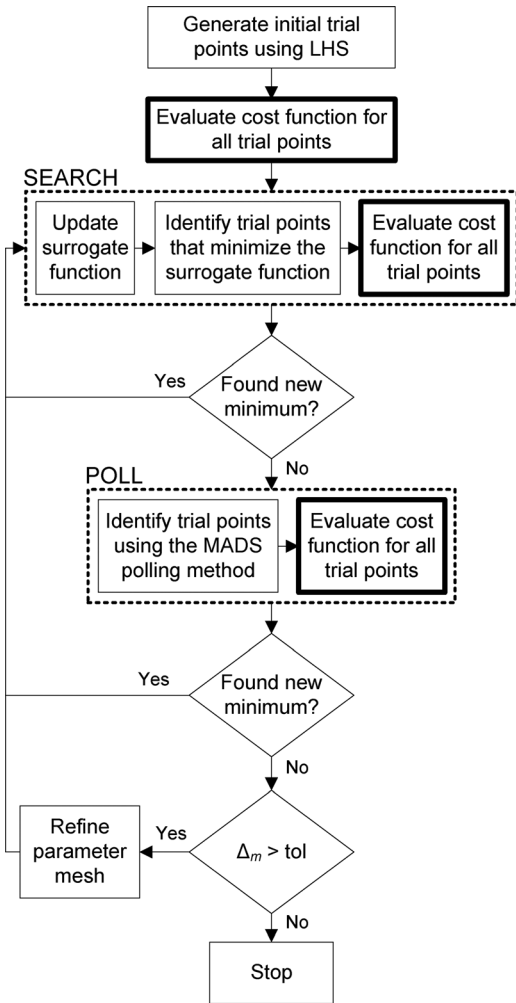


Fig. 3 Flow chart of the SMF optimization routine. Each bolded box indicates a point in the routine where the cost function for a stent design is evaluated. The optimization stops when the size of the discrete parameter mesh (Δ_m) is refined beyond a user specified tolerance (tol).

the SEARCH step fails to improve the current best point, a POLL step is performed. MADS is used to identify a set of $n + 1$ positively spanning POLL points that neighbor the current minimizing point, where n is the number of parameters [30]. If the POLL step succeeds in improving the current best point, the algorithm returns to the SEARCH step. If the POLL step is not successful, then a mesh local optimizer has been found, and the optimization algorithm will either be complete, or the parameter mesh will be refined. In this investigation, refining the parameter space decreased the parameter mesh size (Δ_m) by $[1/4]$. When the POLL step fails and the parameter mesh has been refined to the specified tolerance, the optimization algorithm stops.

While the SMF is capable of optimizing several design parameters, in this investigation each optimization only allowed one parameter to vary. To optimize the N_C , the initial parameter mesh was defined to include all possible integer values. We did not refine the parameter mesh because N_C is not a continuous variable. For the second set of optimizations, the intrastrut angle was a continuous variable, therefore initial parameter meshes were defined to have a spacing of 8 deg and we allowed for three refinements, resulting in a final parameter mesh resolution of 0.5 deg.

To fully automate the optimization routine, the optimization algorithm was coupled to the cost function evaluation using the Tool Command Language (TCL) scripting capabilities within Simvascular (www.simtk.org). The scripts, called external pro-

grams, to execute the optimization algorithm (MATLAB), build models (SolidWorks), perform CFD, and compute cost values (VTK). Because MeshSim is directly integrated into Simvascular, meshing and prescribing boundary conditions was performed using built-in Simvascular subroutines. The majority of the optimization routine was executed on a standard personal computer except for the CFD simulations, which were performed on a high performance computing cluster with 1024 cores, 3 Gb RAM/core, and InfiniBand interconnects (each CFD simulation used 50–100 cores). Because the SMF algorithm allows for multiple cost function values to be computed in parallel, such as during the LHS and POLL steps, the cluster was used to perform multiple CFD simulations simultaneously for increased efficiency.

3 Results

3.1 Optimization of the Number of Circumferentially Repeating Stent Cells. The number of circumferential repeating cells was optimized for stent designs with intrastrut areas of 1 mm^2 , 2 mm^2 , and 3 mm^2 in both large and small vessel models. The optimal design parameters are summarized in Table 1. For stent designs with equivalent intrastrut areas, the optimal number of circumferential repeating cells increased with the increased vessel size, and the optimal cost was lower in the small diameter vessel (e.g., SV-1 mm^2 : $N_C = 7$, $J = 0.590$ versus LV-1 mm^2 : $N_C = 9$, $J = 0.613$). Within vessels of the same diameter, the optimal cost decreased with the increased intrastrut area (e.g., SV-1 mm^2 : $J = 0.590$ versus SV-2 mm^2 : $J = 0.500$). Each optimization converged on an optimal design using seven or fewer function evaluations.

Plots of the cost function versus the number of circumferentially repeating cells and corresponding intrastrut angles are shown in Fig. 4. A visual inspection of intrastrut TAWSS distributions (Fig. 4) indicates that designs with less than the optimal number of repeating circumferential units exhibited greater areas of low TAWSS as a result of struts that are more misaligned with the primary direction of flow and decreased cell axial length. Conversely, in stent designs with greater than the optimal number of circumferentially repeating cells, the increased proximity of adjacent struts decreased the near wall blood flow velocity, and subsequently, TAWSS, within the intrastrut region.

3.2 Optimization of Intrastrut Angle. When the intrastrut angle was allowed to continuously vary, the optimal θ was found to be between 38.5 deg and 46 deg for all stent designs. This result indicates that the optimal intrastrut angle is largely independent of the vessel size and intrastrut area. Plots of the design cost relative to the intrastrut angle are shown in Fig. 5 (black lines). For comparison, the cost from the optimization of the number of circumferentially repeating cells is also shown in Fig. 5 (gray lines). The optimal number of circumferentially repeating cells (Fig. 5, gray circles) corresponds to the stent design closest to the optimal intrastrut angle, indicating that the intrastrut angle dictates the optimal number of circumferentially repeating units.

Table 1 Results from optimizing the number of circumferentially repeating stent cells

Stent design	Cost (J)	Circumferential repetitions (N_C)	Number of function evaluations
SV ($\varnothing = 2.25 \text{ mm}$)			
1 mm^2	0.590	7	6
2 mm^2	0.500	5	6
3 mm^2	0.461	4	4
LV ($\varnothing = 3.0 \text{ mm}$)			
1 mm^2	0.613	9	7
2 mm^2	0.520	7	5
3 mm^2	0.477	6	5

Note: SV = small vessel; LV = large vessel.

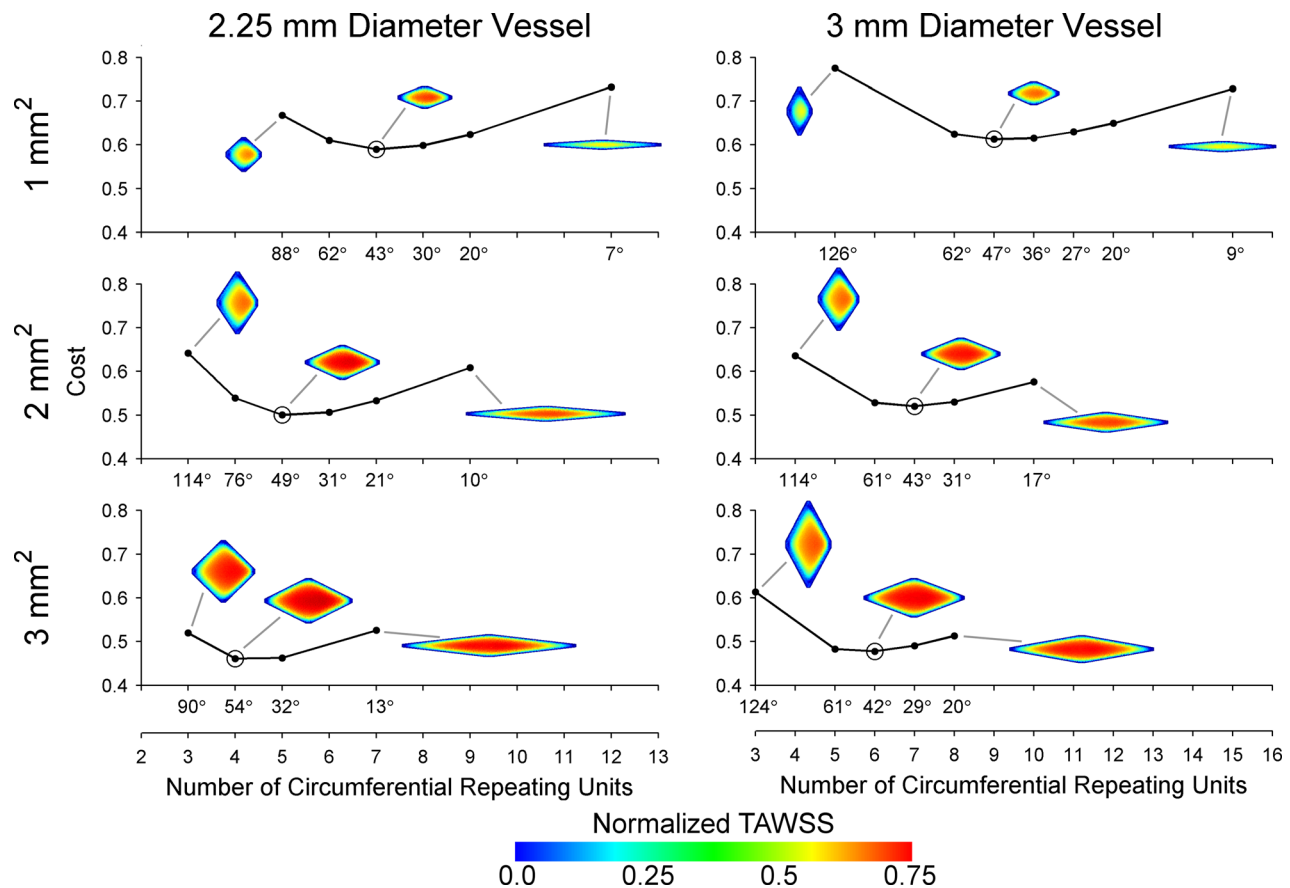


Fig. 4 The cost function versus the number of repeating circumferential units for stent models with various intrastrut areas in a small vessel (left) and large vessel (right). The intrastrut angle corresponding to the number of repeating units is denoted on the individual plot axes for each design and the optimal design is circled on each plot. Patterns of normalized TAWSS_{IS} are shown for the least, most, and optimal number of circumferential repeating units.

The convergence history for the optimization of the intrastrut angle is shown in Fig. 6. The LHS accounted for the first three function evaluations. Although the optimization method allowed for three mesh refinements, all optimization runs converged with less than 20 function evaluations, with the majority of runs only requiring 10 to 15 function evaluations.

4 Discussion

Stent design and geometry are known to influence clinical outcomes including endothelialization and restenosis after DES and BMS implantation, respectively [10,20,33–35], however, previous studies have largely employed a “trial-and-error” approach to improving stent design. In this investigation, we present a robust and computationally efficient methodology for optimizing cardiovascular stent design in an unsteady flow using CFD. The application of the optimization produced two novel findings pertaining to the optimal design of a generic slotted-tube stent. The optimal number of circumferential repeating stent cells is dependent on the intrastrut angle, and the optimal intrastrut angle is independent of both vessel size and the intrastrut area of the stent cell. Since the inflow rate to the model was kept constant for both of the vessel diameters in this investigation, it can be concluded that the optimal intrastrut angle is also independent of the magnitude of the WSS.

The current results confirm and extend the findings of previous stent CFD studies. In a previous study of stent foreshortening, stents with intrastrut angles of 58 deg, 68 deg, and 78 deg were constructed, and it was determined that stents with struts more aligned with the primary direction of flow decrease the area of low WSS [15]. Because angles of less than 58 deg were not tested, this study was unable to determine that further decreases in

the intrastrut angles (<40°) would actually increase the area of low WSS, as was shown in this investigation. Numerous two-dimensional and three-dimensional studies have also found that increasing the axial distance between struts, effectively increasing the intrastrut area, is hemodynamically advantageous, since it allows for a greater area of flow reattachment between the struts [7,8,35,36]. In the current results, this trend was also demonstrated among stent designs in vessels with the same diameter. For these models, the cost function decreased for designs with a greater intrastrut area, indicating that a greater intrastrut area is hemodynamically advantageous.

The cost function in the current investigation measured the disparity in the TAWSS between the stented region and the unstented region. While this cost function is representative of the well-established concept of WSS homeostasis, the actual value of this index has not been previously studied or correlated to vascular disease. Other CFD studies have used a critical value of 5 dynes/cm² as a threshold of low WSS [5,8,11,37,38], since it has been correlated to intimal thickening [39]. However, using 5 dynes/cm² as the threshold may not be able to differentiate between device designs in flow environments with excessively high or low WSS. The cost function used in this investigation is more versatile than a thresholding cost function and is capable of discriminating between stent designs regardless of the flow environment.

Although we performed an unconstrained optimization using a single cost function in this investigation, it is worth noting that the SMF optimization algorithm can be adapted to perform the constrained optimization using a filter method [40,41]. Employing constrained optimization would allow multiple stent design criteria to be simultaneously examined using a constraint violation function in addition to a cost function. This approach is particularly useful for

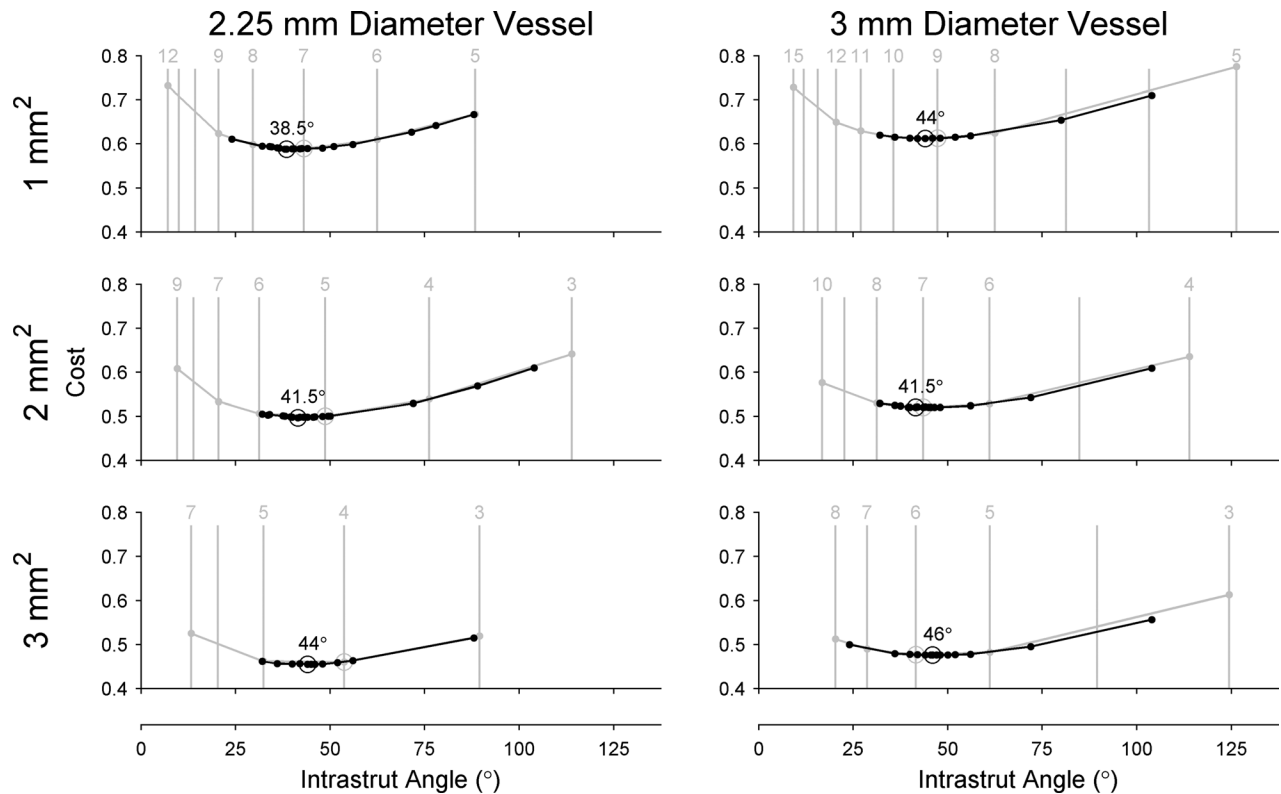


Fig. 5 The cost function versus the intrastrut angle for stent models with various intrastrut areas in a small vessel and large vessel (black lines). The intrastrut angles that correspond to feasible stent designs are shown as vertical lines (gray). The cost function versus the number of circumferentially repeating stent cells is plotted along the gray lines and the number of circumferentially repeating cells is denoted above the lines for models that have been evaluated. Optimal stent designs are circled on all plots.

exploring design trade-offs between the objective function and constraints. In addition, multiple objectives or constraints can be lumped together as a weighted sum, or formal bi-objective optimization can be performed. Yang et al. recently used a constrained SMF method to analyze the relationship between the energy efficiency and WSS when optimizing the shape of a Fontan surgical design [42]. With regard to stent hemodynamics, constrained optimization could be used to examine the trade-offs between low WSS and other hemodynamic indices thought to be related to restenosis, such as the oscillatory shear index, spatial, or temporal wall shear-stress gradients, and the wall shear stress angle gradients [14,43–45].

The use of constrained optimization would be particularly interesting to study the relationship between hemodynamic and nonhemodynamic stent design criteria. For example, the strut thickness was kept constant in this investigation because optimizing this

parameter from a purely hemodynamic perspective produces a stent design with a negligible thickness. However, if a constraint violation function was formulated based on radial stiffness, it is likely that the competing solid mechanic and hemodynamic effects of reducing the strut thickness would prevent the optimization from converging on an infeasible design. Other solid mechanics constraints might include luminal gain, stress induced on the arterial wall, and flexibility [46–50]. When designing DESs, the uniformity of the drug elution could also be considered since non-uniform drug concentrations resulting from stent geometry or overlapping stents has previously been shown to suppress re-endothelialization atop stent struts [35,51].

The current results should be interpreted within the constraints of several potential limitations. All CFD simulations employed a rigid wall assumption. Stent implantation has been shown to decrease the arterial compliance to zero [21]. Thus, it is unlikely that this

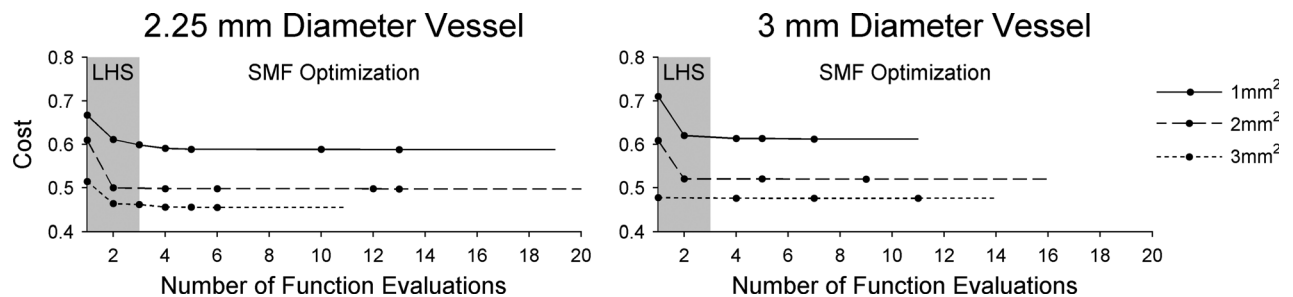


Fig. 6 Convergence history for the optimization of the intrastrut angle for stent models with various intrastrut areas in a small vessel and large vessel. The Latin hypercube sampling (LHS) portion of the optimization routine is shaded in gray. The surrogate management framework (SMF) represents the portion of the optimization algorithm that used alternating SEARCH and POLL steps to converge on the optimal stent design.

assumption influenced the CFD results within the stented region. In the proximal and distal portions of the CFD models, the inclusion of deformable walls would likely decrease the TAWSS due to cyclic increases in vessel diameter. This would alter the computed cost values, however, the optimization results would likely not be affected since the relative cost between stent designs would be similar to the current results. The present results were obtained assuming a circular cross-section within the stent region of the vessel. However, previous studies indicate that stent implantation may induce circumferential straightening, or prolapse, of the vessel between struts to give the vessel a more polygonal shape [20]. The effect of including prolapse in the CFD models is unknown since various models of prolapse have shown both an increase in intra-strut WSS [52] and a decrease in intra-strut WSS [38]. Therefore, the inclusion of prolapse in the CFD likely depends on the stent design and the methodology implemented. In this investigation, vessel prolapse would have the most pronounced effect in models with large intra-strut areas and a small number of circumferentially repeating stent cells. In models with smaller intra-strut areas and a large number of circumferentially repeating cells, the deviation from a circular cross-section would be less pronounced [20]. In comparison to the current stent models, inclusion of prolapse in these models would likely increase the TAWSS in the center of the intra-strut area and decrease the TAWSS near the stent struts.

The current investigation only considered a generic slotted-tube stent design and the designs of the most commonly used stents are more intricate. Nevertheless, the current results can likely be translated to similar closed-cell or open-cell stent designs with peak-to-peak connections, such as the Driver stent platform (Medtronic CardioVascular, Santa Rosa, CA). Stent designs with peak-to-valley connections, coil designs, and stents with more elaborate connections will require further analysis to optimize their unique geometries and will be the focus of our future investigations in this area.

In summary, the current investigation describes an efficient optimization framework that uses CFD to determine hemodynamically optimal coronary stents. The method was applied to determine the number of circumferentially repeating stents cells and intra-strut angles that minimize the area of low TAWSS. The current results suggest that slotted-tube stent designs with an intra-strut angle of about 40 deg are hemodynamically optimal, regardless of the vessel size and intra-strut area. Incorporating the results of this investigation in future stent designs may improve endothelialization after DESs and reduce neointimal hyperplasia and subsequent restenosis after BMS.

Acknowledgment

This work is supported by a Translational Opportunity Grant of the Pilot and Collaborative Clinical and Translational Research Grants program from the Clinical and Translational Science Institute of Southeastern Wisconsin and a Burroughs Wellcome Fund Career Award at the Scientific Interface to ALM. Computational support for this work was made possible by NSF Grant Nos. OCI-0923037 and CBET-0521602. The authors recognize Nathan Wilson, Ph.D., of Open Source Medical Software Corporation for technical assistance.

References

- [1] Doyle, B., Rihal, C. S., O'Sullivan, C. J., Lennon, R. J., Wiste, H. J., Bell, M., Bresnahan, J., and Holmes, D. R., 2007, "Outcomes of Stent Thrombosis and Restenosis During Extended Follow-Up of Patients Treated With Bare-Metal Coronary Stents," *Circulation*, **116**(21), pp. 2391–2398.
- [2] James, S. K., Stenestrand, U., Lindbäck, J., Carlsson, J., Scherstén, F., Nilsson, T., Wallentin, L., Lagerqvist, B., and Group, S. S., 2009, "Long-Term Safety and Efficacy of Drug-Eluting Versus Bare-Metal Stents in Sweden," *N. Engl. J. Med.*, **360**(19), pp. 1933–1945.
- [3] Stone, G. W., Rizvi, A., Sudhir, K., Newman, W., Applegate, R. J., Cannon, L. A., Maddux, J. T., Cutlip, D. E., Simonton, C. A., Sood, P., Kereiakes, D. J., and Investigators, S. I., 2011, "Randomized Comparison of Everolimus- and Paclitaxel-Eluting Stents. 2-Year Follow-Up From the SPIRIT (Clinical Evaluation of the XIENCE V Everolimus Eluting Coronary Stent System) IV Trial," *J. Am. Coll. Cardiol.*, **58**(1), pp. 19–25.

- [4] Leon, M. B., Kandzari, D. E., Eisenstein, E. L., Anstrom, K. J., Mauri, L., Cutlip, D. E., Nikolsky, E., O'Shaughnessy, C., Overlie, P. A., Kirtane, A. J., McLaurin, B. T., Solomon, S. L., Douglas, J. S., Popma, J. J., and Investigators, E. I., 2009, "Late Safety, Efficacy, and Cost-Effectiveness of a Zotarolimus-Eluting Stent Compared With a Paclitaxel-Eluting Stent in Patients With De Novo Coronary Lesions: 2-Year Follow-Up From the ENDEAVOR IV Trial (Randomized, Controlled Trial of the Medtronic Endeavor Drug [ABT-578] Eluting Coronary Stent System Versus the Taxus Paclitaxel-Eluting Coronary Stent System in De Novo Native Coronary Artery Lesions)," *JACC Cardiovasc. Interv.*, **2**(12), pp. 1208–1218.
- [5] Finn, A. V., Nakazawa, G., Joner, M., Kolodgie, F. D., Mont, E. K., Gold, H. K., and Virmani, R., 2007, "Vascular Responses to Drug Eluting Stents: Importance of Delayed Healing," *Arterioscler., Thromb., Vasc. Biol.*, **27**(7), pp. 1500–1510.
- [6] Joner, M., Nakazawa, G., Finn, A. V., Quee, S. C., Coleman, L., Acampado, E., Wilson, P. S., Skorjia, K., Cheng, Q., Xu, X., Gold, H. K., Kolodgie, F. D., and Virmani, R., 2008, "Endothelial Cell Recovery Between Comparator Polymer-Based Drug-Eluting Stents," *J. Am. Coll. Cardiol.*, **52**(5), pp. 333–342.
- [7] Kotani, J., Awata, M., Nanto, S., Uematsu, M., Oshima, F., Minamiguchi, H., Mintz, G. S., and Nagata, S., 2006, "Incomplete Neointimal Coverage of Sirolimus-Eluting Stents: Angioscopic Findings," *J. Am. Coll. Cardiol.*, **47**(10), pp. 2108–2111.
- [8] LaDisa, J. F., Olson, L. E., Molthen, R. C., Hettrick, D. A., Pratt, P. F., Hardel, M. D., Kersten, J. R., Warltier, D. C., and Pagel, P. S., 2005, "Alterations in Wall Shear Stress Predict Sites of Neointimal Hyperplasia After Stent Implantation in Rabbit Iliac Arteries," *Am. J. Physiol. Heart Circ. Physiol.*, **288**(5), pp. H2465–2475.
- [9] and Liu, S. Q. and Goldman, J., 2001, "Role of Blood Shear Stress in the Regulation of Vascular Smooth Muscle Cell Migration," *IEEE Trans. Biomed. Eng.*, **48**(4), pp. 474–483.
- [10] Sprague, E. A., Luo, J., and Palmaz, J. C., 2000, "Endothelial Cell Migration Onto Metal Stent Surfaces Under Static and Flow Conditions," *J. Long Term Eff. Med. Implants*, **10**(1–2), pp. 97–110. Available at <http://dl.begellhouse.com/journals/1bef42082d7a0fd1,10a09db02be3aae4,2689d22927f48a2a.html>.
- [11] LaDisa, J. F., Olson, L. E., Guler, I., Hettrick, D. A., Audi, S. H., Kersten, J. R., Warltier, D., and C.Pagel, P. S., 2004, "Stent Design Properties and Deployment Ratio Influence Indexes of Wall Shear Stress: A Three-Dimensional Computational Fluid Dynamics Investigation Within a Normal Artery," *J. Appl. Physiol.*, **97**(1), pp. 424–430.
- [12] He, Y., Duraiswamy, N., Frank, A. O., and Moore, J. E., 2005, "Blood Flow in Stented Arteries: A Parametric Comparison of Strut Design Patterns in three Dimensions," *ASME J. Biomech. Eng.*, **127**(4), pp. 637–647.
- [13] Duraiswamy, N., Schoepfoerster, R. T., and Moore, J. E., 2009, "Comparison of Near-Wall Hemodynamic Parameters in Stented Artery Models," *ASME J. Biomech. Eng.*, **131**(6), p. 061006.
- [14] Murphy, J. B. and Boyle, F. J., 2010, "A Full-Range, Multi-Variable, CFD-Based Methodology to Identify Abnormal Near-Wall Hemodynamics in a Stented Coronary Artery," *Biorheology*, **47**(2), pp. 117–132.
- [15] LaDisa, J. F., Olson, L. E., Hettrick, D. A., Warltier, D. C., Kersten, J. R., and Pagel, P. S., 2005, "Axial Stent Strut Angle Influences Wall Shear Stress After Stent Implantation: Analysis Using 3D Computational Fluid Dynamics Models of Stent Foreshortening," *Biomed. Eng. Online*, **4**, p. 59.
- [16] Gundert, T. J., Shadden, S. C., Williams, A. R., Koo, B. K., Feinstein, J. A., and LaDisa, J. F., 2011, "A Rapid and Computationally Inexpensive Method to Virtually Implant Current and Next-Generation Stents into Subject-Specific Computational Fluid Dynamics Models," *Ann. Biomed. Eng.*, **39**(5), pp. 1423–1437.
- [17] Blouza, A., Dumas, L., and M'Baye, I., 2008, "Multiobjective Optimization of a Stent in a Fluid-Structure Context," Proceedings of the 2008 GECCO Conference Companion on Genetic and Evolutionary Computation, ACM, Atlanta, GA, USA, pp. 2055–2060.
- [18] Srinivas, K., Nakayama, T., Ohta, M., Obayashi, S., and Yamaguchi, T., 2008, "Studies on Design Optimization of Coronary Stents," *ASME J. Med. Devices*, **2**(1), p. 011004.
- [19] Atherton, M. A. and Bates, R. A., 2004, "Robust Optimization of Cardiovascular Stents: A Comparison of Methods," *Eng. Optimiz.*, **36**(2), pp. 207–217.
- [20] Garasic, J. M., Edelman, E. R., Squire, J. C., Seifert, P., Williams, M. S., and Rogers, C., 2000, "Stent and Artery Geometry Determine Intimal Thickening Independent of Arterial Injury," *Circulation*, **101**(7), pp. 812–818. Available at <http://circ.ahajournals.org/content/101/7/812>.
- [21] LaDisa, J. F., Hettrick, D. A., Olson, L. E., Guler, I., Gross, E. R., Kress, T. T., Kersten, J. R., Warltier, D. C., and Pagel, P. S., 2002, "Stent Implantation Alters Coronary Artery Hemodynamics and Wall Shear Stress During Maximal Vasodilation," *J. Appl. Physiol.*, **93**(6), pp. 1939–1946.
- [22] Vignon-Clementel, I. E., Alberto Figueroa, C., Jansen, K. E., and Taylor, C. A., 2006, "Outflow Boundary Conditions for Three-Dimensional Finite Element Modeling of Blood Flow and Pressure in Arteries," *Comput. Methods Appl. Mech. Eng.*, **195**(29–32), pp. 3776–3796.
- [23] Ellwein, L., Otake, H., Gundert, T., Koo, B.-K., Shinke, T., Honda, Y., Shite, J., and LaDisa, J., 2011, "Optical Coherence Tomography for Patient-Specific 3D Artery Reconstruction and Evaluation of Wall Shear Stress in a Left Circumflex Coronary Artery," *Cardiovasc. Eng. Technol.*, **2**(3), pp. 212–227.
- [24] Williams, A. R., Koo, B. K., Gundert, T. J., Fitzgerald, P. J., and LaDisa, J. F., 2010, "Local Hemodynamic Changes Caused by Main Branch Stent Implantation and Subsequent Virtual Side Branch Balloon Angioplasty in a Representative Coronary Bifurcation," *J. Appl. Physiol.*, **109**(2), pp. 532–540.
- [25] Tang, B., Cheng, C., Draney, M., Wilson, N., Tsao, P., Herfkens, R., and Taylor, C., 2006, "Abdominal Aortic Hemodynamics in Young Healthy Adults at Rest and During Lower Limb Exercise: Quantification Using Image-Based

- Computer Modeling," *Am. J. Physiol. Heart Circ. Physiol.*, **291**(2), pp. H668–H676.
- [26] Glagov, S., Weisenberg, E., Zarins, C. K., Stankunavicius, R., and Koletlis, G. J., 1987, "Compensatory Enlargement of Human Atherosclerotic Coronary Arteries," *N. Engl. J. Med.*, **316**(22), pp. 1371–1375.
- [27] Kamiya, A. and Togawa, T., 1980, "Adaptive Regulation of Wall Shear Stress to Flow Change in the Canine Carotid Artery," *Am. J. Physiol. Heart Circ. Physiol.*, **239**(1), pp. H14–H21. Available at <http://ajpheart.physiology.org/content/239/1/H14.abstract>.
- [28] Booker, A. J., Dennis, J. E., Frank, P. D., Serafini, D. B., Torczon, V., and Trosset, M. W., 1999, "A Rigorous Framework for Optimization of Expensive Functions by Surrogates," *Struct. Multidiscip. Optimiz.*, **17**(1), pp. 1–13.
- [29] Marsden, A. L., Feinstein, J. A., and Taylor, C. A., 2008, "A Computational Framework for Derivative-Free Optimization of Cardiovascular Geometries," *Comput. Methods Appl. Mech. Eng.*, **197**(21–24), pp. 1890–1905.
- [30] Audet, C. and Dennis, J. J. E., 2006, "Mesh Adaptive Direct Search Algorithms for Constrained Optimization," *SIAM J. Optim.*, **17**(1), pp. 188–217.
- [31] Lophaven, S., Nielsen, H., Søndergaard, J., 2002, "DACE - A MATLAB Kriging Toolbox Version 2.0," Technical University of Denmark, Copenhagen, Technical Report IMM-TR-2002-12M.
- [32] McKay, M. D., Beckman, R. J., and Conover, W., 1979, "A Comparison of Three Methods for Selecting Values of Input Variables in the Analysis of Output from a Computer Code," *Technometrics*, **21**(2), pp. 239–245.
- [33] Rogers, C. and Edelman, E. R., 1995, "Endovascular Stent Design Dictates Experimental Restenosis and Thrombosis," *Circulation*, **91**(12), pp. 2995–3001. Available at <http://circ.ahajournals.org/content/91/12/2995.short>.
- [34] Pache, J., Kastrati, A., Mehilli, J., Schühlen, H., Dotzer, F., Hausleiter, J., Fleckenstein, M., Neumann, F. J., Sattelberger, U., Schmitt, C., Müller, M., Dirschinger, J., and Schömig, A., 2003, "Intracoronary Stenting and Angiographic Results: Strut Thickness Effect on Restenosis Outcome (ISAR-STERO-2) Trial," *J. Am. Coll. Cardiol.*, **41**(8), pp. 1283–1288.
- [35] Finn, A. V., Kolodgie, F. D., Harnek, J., Guerrero, L. J., Acampado, E., Tefera, K., Skorija, K., Weber, D. K., Gold, H. K., and Virmani, R., 2005, "Differential Response of Delayed Healing and Persistent Inflammation at Sites of Overlapping Sirolimus- or Paclitaxel-Eluting Stents," *Circulation*, **112**(2), pp. 270–278.
- [36] LaDisa, J. F., Guler, I., Olson, L. E., Hettrick, D. A., Kersten, J. R., Warltier, D. C., and Pagel, P. S., 2003, "Three-Dimensional Computational Fluid Dynamics Modeling of Alterations in Coronary Wall Shear Stress Produced by Stent Implantation," *Ann. Biomed. Eng.*, **31**(8), pp. 972–980.
- [37] Balossino, R., Gervaso, F., Migliavacca, F., and Dubini, G., 2008, "Effects of Different Stent Designs on Local Hemodynamics in Stented Arteries," *J. Biomech.*, **41**(5), pp. 1053–1061.
- [38] LaDisa, J. F., Olson, L. E., Guler, I., Hettrick, D. A., Kersten, J. R., Warltier, D. C., and Pagel, P. S., 2005, "Circumferential Vascular Deformation After Stent Implantation Alters Wall Shear Stress Evaluated With Time-Dependent 3D Computational Fluid Dynamics Models," *J. Appl. Physiol.*, **98**(3), pp. 947–957.
- [39] Ku, D. N., Giddens, D. P., Zarins, C. K., and Glagov, S., 1985, "Pulsatile Flow and Atherosclerosis in the Human Carotid Bifurcation. Positive Correlation Between Plaque Location and Low Oscillating Shear Stress," *Arteriosclerosis*, **5**(3), pp. 293–302.
- [40] Fletcher, R. and Leyffer, S., 2002, "Nonlinear Programming Without a Penalty Function," *Math. Program.*, **91**(2), pp. 239–269.
- [41] Audet, C. and Dennis, J. J. E., 2004, "A Pattern Search Filter Method for Nonlinear Programming Without Derivatives," *SIAM J. Optim.*, **14**(4), pp. 980–1010.
- [42] Yang, W., Feinstein, J. A., and Marsden, A. L., 2010, "Constrained Optimization of an Idealized Y-Shaped Baffle for the Fontan Surgery at Rest and Exercise," *Comput. Methods Appl. Mech. Eng.*, **199**(33–36), pp. 2135–2149.
- [43] Longest, P. W. and Kleinstreuer, C., 2000, "Computational Haemodynamics Analysis and Comparison Study of Arterio-Venous Grafts," *J. Med. Eng. Technol.*, **24**(3), pp. 102–110.
- [44] Lei, M., Kleinstreuer, C., and Truskey, G. A., 1996, "A Focal Stress Gradient-Dependent Mass Transfer Mechanism for Atherogenesis in Branching Arteries," *Med. Eng. Phys.*, **18**(4), pp. 326–332.
- [45] He, X. and Ku, D. N., 1996, "Pulsatile Flow in the Human Left Coronary Artery Bifurcation: Average Conditions," *ASME J. Biomech. Eng.*, **118**(1), pp. 74–82.
- [46] Zahedmanesh, H. and Lally, C., 2009, "Determination of the Influence of Stent Strut Thickness Using the Finite Element Method: Implications for Vascular Injury and In-Stent Restenosis," *Med. Biol. Eng. Comput.*, **47**(4), pp. 385–393.
- [47] Bedoya, J., Meyer, C. A., Timmins, L. H., Moreno, M. R., and Moore, J. E., 2006, "Effects of Stent Design Parameters on Normal Artery Wall Mechanics," *ASME J. Biomech. Eng.*, **128**(5), pp. 757–765.
- [48] Lally, C., Dolan, F., and Prendergast, P. J., 2005, "Cardiovascular Stent Design and Vessel Stresses: A Finite Element Analysis," *J. Biomech.*, **38**(8), pp. 1574–1581.
- [49] Ako, J., Bonneau, H. N., Honda, Y., and Fitzgerald, P. J., 2007, "Design Criteria for the Ideal Drug-Eluting Stent," *Am. J. Cardiol.*, **100**(8B), pp. 3M–9M.
- [50] Timmins, L. H., Moreno, M. R., Meyer, C. A., Criscione, J. C., Rachev, A., and Moore, J. E., 2007, "Stented Artery Biomechanics and Device Design Optimization," *Med. Biol. Eng. Comput.*, **45**(5), pp. 505–513.
- [51] Balakrishnan, B., Tzafiriri, A. R., Seifert, P., Groothuis, A., Rogers, C., and Edelman, E. R., 2005, "Strut Position, Blood Flow, and Drug Deposition: Implications for Single and Overlapping Drug-Eluting Stents," *Circulation*, **111**(22), pp. 2958–2965.
- [52] Murphy, J. and Boyle, F., 2008, "Assessment of the Effects of Increasing Levels of Physiological Realism in the Computational Fluid Dynamics Analyses of Implanted Coronary Stents," *IEEE Conf. Proc. Eng. Med. Biol. Soc.*, **2008**, pp. 5906–5909.